Structural and optical properties of tin (II) sulfide thin films deposited using organophosphorus precursor (Ph_3PS)

Kawther Assili[a,b], Khaled Alouani[a] and Xavier Vilanova[b]

a) University of Tunis El-Manar, Faculty of Science, Laboratory of Analytical Chemistry and Electrochemistry, Faculty of Science, Campus, 2092, Tunis, Tunisia.

b) University Rovira i Virgili, Department of Electronic, Electrical and Automatic Engineering, 43007, Tarragona, Spain.

Graphical abstract

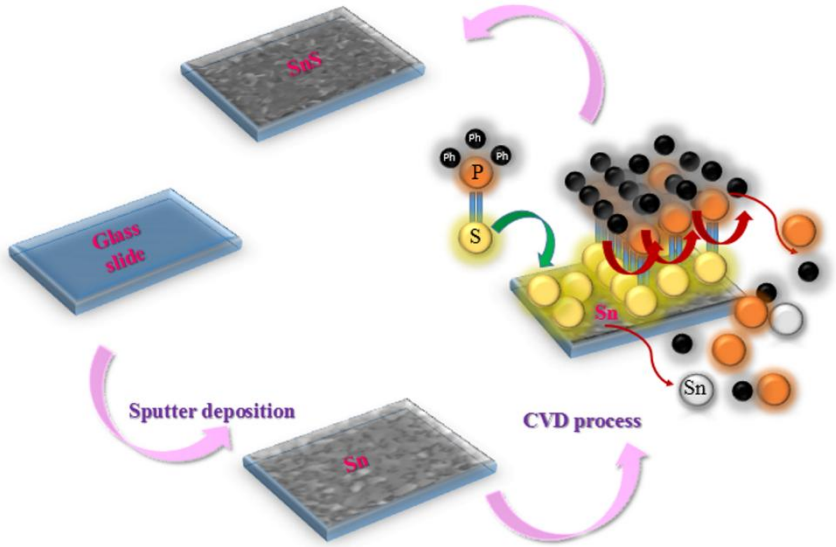

Highlights

- Tin sulfide thin films were successfully prepared using organophosphorus precursor.
- Structural properties were investigated as a function of sulphidisation temperature.
- Optical absorption measurements show a direct optical band gap.
- This cheap material could be useful for optoelectronic applications.

Abstract

Tin sulfide (SnS) thin films have been deposited onto glass substrates using Triphenylphosphine sulfide (Ph_3PS) as a sulfur precursor in a CVD reactor in a temperature range of 250-400 °C. The influence of the sulphidisation temperature in the crystal structure, surface morphology, chemical composition and optical properties has been investigated. X-ray diffraction, energy dispersive analysis of X-rays, and Raman spectroscopy showed that pure SnS thin films have been successfully obtained at 250 °C. All the deposited films were polycrystalline and showed orthorhombic structure, with a preferential orientation according to the direction <111>.

The optical measurements showed that the films deposited exhibited a direct allowed transition and have a relatively high absorption coefficient. The presence of mixed tin sulfide phases granted by the variation of the sulphidisation temperature has affected the optical properties of the deposited films. The refractive index (n) and extinction coefficient (k), has low values compared to conventional semiconductor materials. The grown films can be considered as a good light absorbing material and a promising candidate for application in optoelectronic devices.

Keywords: Thin films, SnS, Triphenylphosphine sulfide, Chemical vapor deposition, XRD, Optical constants.

1. Introduction

Binary metal sulfide semiconductors such as ZnS [1], Ag_2S [2], Sb_2S_3 [3] and others [4-6] have attracted the attention of many investigators due to their advantageous structures and nanostructures and their high chemical and thermal stability [7, 8]. Most of these semiconductor sulfides exhibit a narrow band-gap, which makes them potential candidates for applications in the field of solar cells [9] and as thin film electrodes [10]. Recently, these binary sulfides have been used in other application areas such as gas sensors [11] and opto-electronic devices [12]. These metal sulfide thin films are usually obtained using both physical and chemical methods such as sputtering [13], molecular beam epitaxy [14], laser ablation [15], spray pyrolysis [16], electrochemical deposition [17], chemical bath deposition [18], vacuum evaporation [19], thermal evaporation [20], and chemical vapor deposition [21]. Among all of these methodologies, the chemical vapor deposition (CVD) allows obtaining a very good film

uniformity and excellent adhesion, as well as controlling the crystal structure and film morphology by adjusting the working temperature and deposition rate. In fact, several types of CVD have been introduced in the past years according to the precursors used and the deposition conditions [22].

One of the metal sulfides that have attracted high interest in the past years is the tin sulfide (Sn_xS_y), since thin films of this sulfide have shown potential applications in various fields like electric switching [23], photovoltaic conversion devices [24] lithium batteries [25] and gas detector [26]. Besides, this is an interesting material due to its ecological and economical fabrication as well as its abundancy [27,28].

This binary compound, that belong to IV-VI type of semiconductor materials, can be present in a variety of forms, including the grey SnS (1.3 eV) [29], the yellow SnS_2 (2.17 eV) [30], and the brown Sn_2S_3 (0.95 eV) [31]. Among them, SnS with orthorhombic crystals has attracted a considerable attention due to valuable characteristics. It has a high fundamental absorption coefficient (larger than 10^4 cm^{-1}) [26] and a bandgap in the range of 1.3 - 1.4 eV [30], which allows him to exhibit a high conversion efficiency, up to 25%, in photovoltaic devices, similar to the one found for silicon films [32]. Previous works have shown that the SnS usually exhibits a p-type conduction [33], with an electrical resistivity of 32.9 Ω.cm [34].

Many sulfur precursors have been used for the synthesis of tin sulfide, including: $SnCl_2$, Na_2S or $(NH_4)_2S$ from aqueous solution [35] and more recently, the compounds containing a M-S bond such as $[(CF_3CH_2S)_4Sn]$ [25] and $[M(E_2CNR_2)_2]$, (M= Metal, R= *n*-Bu, Et and E= S) [36]. Boudjouk et al. have also used Benzyl-substituted tin chalcogenides like $[(Bn_3Sn)_2S]$ $[(Bn_2SnS)_3]$ [37] and $(Ph_3Sn)_2S$ [38] as a single-source precursors.

Despite the susceptibility of these precursor to produce thin films with high quality and interesting properties, the main disadvantages with most of those procedures is the use or the formation of products with high volatility and toxicity, like the elemental sulfur, H_2S, SO_2 or SO_3 [38]. An approach to alleviate these disadvantages is to avoid these compounds and replace them with stable and non-toxic precursors. One proposed precursor to replace those compounds is the Triphenylphosphine sulfide (Ph_3PS). To the best of our knowledge, it is the first time that this monodentate organophosphorus compound has been used to produce tin monosulfide (SnS) thin films.

In the following, we investigate the deposition of tin sulfide thin films by chemical vapor deposition (CVD) process using a new sulfur precursor, the Triphenylphosphine sulphide. We checked the structural and morphological properties of the deposited films depending on the

variation of sulphidisation temperature in the range of 250-400 °C. Optical constants such as absorption coefficient, band gap energy, refractive index, extinction coefficient and dielectric constants were computed in order to set the optical performance of the deposited films.

2. Experimental procedure

2.1 Substrate preparation

The substrates used for the deposition of the films were microscope slides of glass. The glass slides with 1.2 mm thick were cut into pieces of 1.2 x 1 cm. The glass substrates were cleaned in an ultrasonic bath containing trichloroethylene for 5 min and then rinsed in acetone, ethanol and deionized water. Afterwards, the substrates were dried with a dry air at 99.99% of purity, before being placed in the magnetron sputtering system.

2.2 Sputtering conditions

Layers of tin with 200 nm thickness were deposited by sputtering on the glass substrates using a 2" Sn target (99.99% pure), placed at 35 mm away from the substrate. The sputtering System used is the DC magnetron sputtering system ATC Orion 8-HV from AJA International with a power of 100 W located at the University Rovira i Virgili. The DC sputtering was operated at 3 mTorr of vacuum pressure and the deposition was performed with a 120 sccm flow of Argon during 720 s.

2.3 Chemical vapor deposition of SnS

The substrates covered by tin were placed on a stoneware support inside a CVD system Carbolite model HST 12/600. 100 mg of the triphenylphosphine sulfide ($Ph_3P=S$) were also placed on the same support at a distance of 2 cm from the substrate. Triphenylphosphine sulfide is a very stable molecule which was purchased from Fluka AG and used for the chemical vapor process without further purification.

Since at room temperature both tin and $Ph_3P=S$ precursor are in solid state and at 250 °C both are in gaseous state, we have chosen to carry out the sulphidisation process at temperatures in the range of 250 °C - 400 °C, during 90 min. Therefore, the process can be considered as a V-V method (vapor-vapor). Argon, with a flow of 120 sccm, has been used as a carrier gas. Once the process has been finished, the film has taken out the reactor and cleaned with nitrogen gas in order to remove contamination from the surface. As illustrated in Figure 1, the CVD process is based on a series of events; the first one consist to the formation of the gas phase by

transforming the solid precursors to a vapor product. After a gas phase reaction, the inert carrier gas ensures the transport of the gaseous product to the substrate, where adsorption and subsequent nucleation occurs, leading to the formation of the film. Finally, reaction by-products diffuse out the reactor.

Generally, the CVD lead to a conformal coverage, better than in other techniques such as physical vapor deposition [39].

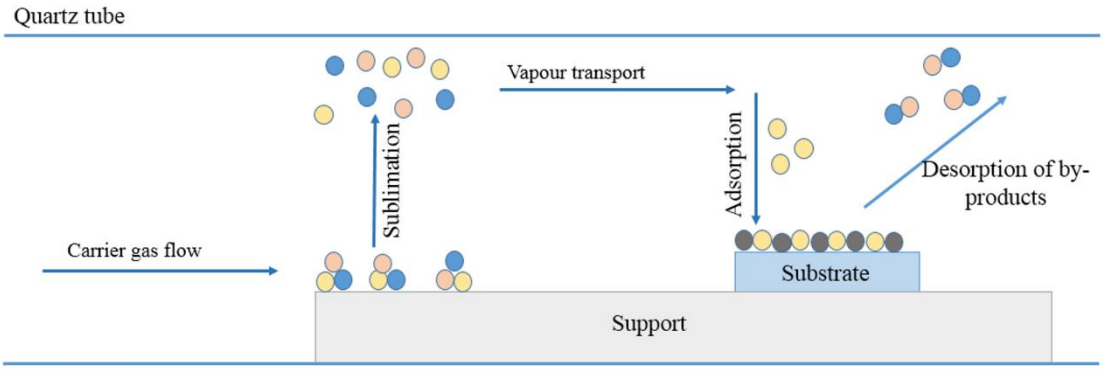

Figure 1. Schematic diagram of CVD deposition

2.4 Characterization techniques

The structural properties of the tin sulfide films were studied by X-ray diffraction technique (XRD). The XRD measurements were performed at room temperature using a Philips (PW1729 system) diffractometer, with a X-ray source (CuKα) wavelength λ = 0.15405 nm. The morphological and compositional characterization of the tin sulfide films were carried out using environmental scanning electron microscopy (ESEM). The environmental scanning electron microscopy used was the ESEM Quanta 600 microscope from FEI company. Raman spectroscopy measurement were recorded at room temperature using Jobin Yovan (T64000) spectrometer. Backscattering geometry was used with excitation of argon laser at 488 nm. The optical transmittance T(λ) and reflectance R (λ) were carried out at room temperature using a VARIAN spectrophotometer over a large spectral range (250–2500 nm).

3. Results and Discussion

3.1 Structural studies

It is noteworthy to mention that, depending on the temperature, the tin monosulfide can crystallize in two main crystal system: The orthorhombic system (α phase), stable at low temperature, which is characterized by the GeS structure type [40] and the pseudo-tetragonal system (β phase), stable at higher temperatures, beyond 800 °C [41].

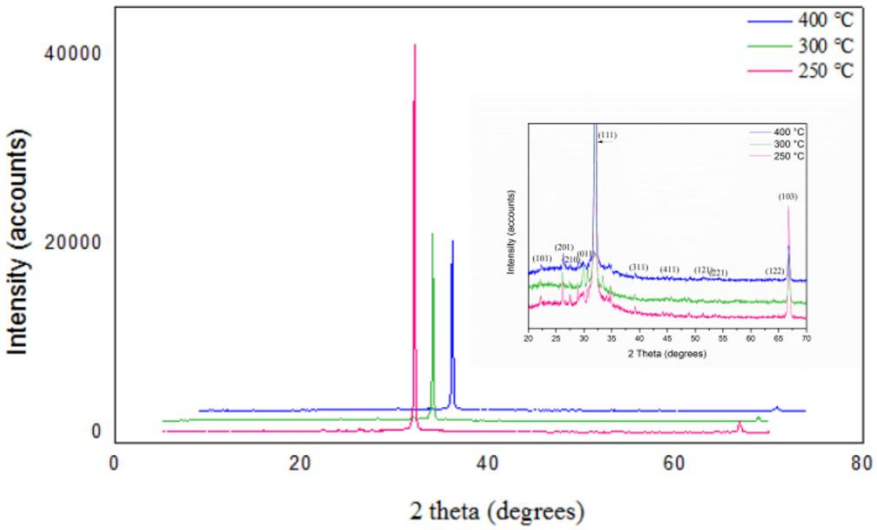

Figure 2. XRD patterns of SnS films on glass substrates at different sulfidisation temperature

Table 1. Comparison of calculated and standard lattice parameters values for the SnS films at different sulphidisation temperatures.

	T = 250 °C	**T = 300 °C**	**T= 400 °C**	**Bibliographic data [40]**
a (Å)	11.015	11.5076	11.3329	10.9575
b (Å)	3.971	3.9519	3.9366	3.9399
c (Å)	4.15	4.2426	4.2420	4.2273

Figure 2 depicts the XRD patterns of SnS films synthesized at different sulphidisation temperatures. All the layers show an intense peak located at 2θ = 32°, with the preferential orientation (111). A zoom of the set of diffractograms, show that other peaks were also observed with comparatively lower intensities, which can be attributed to (101), (201), (011) and (103) planes of SnS phase (inset in Figure 2). The evaluated lattice parameters are summarized in Table 1, and the peaks positions are in good agreement with the JCPDS files (card nos. 04-015-2205) of the orthorhombic SnS phase [40]. This structure with the Pnma space group

characterized by two adjacent double layers stacked along c axis, wherein each sulfur ion is coordinated to three Sn^{2+} ions as shown in the unit cell (Figure 3). According to these results, the films deposited in the temperature range of 250-400 °C are composed mainly by the orthorhombic Tin sulfide. Interestingly, some other diffraction peaks with very low intensity, not associated to SnS, can be identified at ≈ 33°, 34°, 35° and 39°. These peaks could be assigned to Sn_2S_3 (COD 9011236 or COD 2310450), or even to SnS_2 (COD 7038082 show peaks at 33.5 and 33.6 and COD 7038076 show peaks at 34° and 35°). Therefore, other minor tin sulphide phases can be present in the samples.

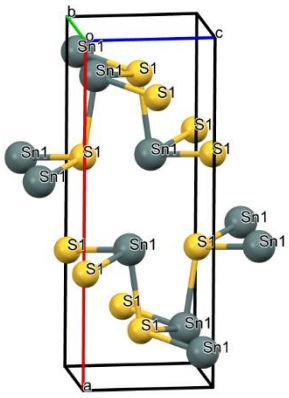

Figure 3. The SnS unit cell scheme.

It can be also observed that, by increasing the sulphidisation temperature, the intensity of the (111) reflection decreases and some of the other reflections are vanishing when growing the film at 400 °C. Tin layers sulfidised at 250°C had the best crystallinity, since the diffraction peak intensities are weakening when increasing the sulphidisation temperatures, which can be related to the crystallite size growth or the thickness of the films. The decrease of the intensity peaks and the disappearance of others in the spectra can also be attributed to the formation of other tin sulfide phases richer in sulfur, such as Sn_2S_3 and SnS_2. However, the very high intensity peaks of SnS phase can mask any minor peak related to other phases, thereby, is very difficult to index the SnS_2 and Sn_2S_3 phases in the XRD pattern. Therefore, other analysis are required to confirm the presence of these other tin sulphide phases.

In order to quantify the preferred orientation of crystallites, the texture coefficient TC (*hkl*) has been calculated using the following relation [42].

$$TC(hkl) = \frac{\frac{I_r(hkl)}{I_0(hkl)}}{\frac{1}{n}\sum \frac{I_r(hkl)}{I_0(hkl)}} \quad (1)$$

where I_r (*hkl*) is the measured relative intensity of a plane (*hkl*), I_o (*hkl*) is the standard intensity of the plane (*hkl*) taken from the JCPDS data (card nos. 04-015-2205) [40], and *n* is the number of diffraction peaks.

Table 2. Values of the the texture coefficient (TC) of (hkl) planes

Temperatures (°C)	**TC (111)**	**TC (101)**	**TC (201)**	**TC (103)**
250	16.010	0.021	0.057	0.294
300	15.994	0.039	0.090	0.305
400	16.043	0.022	0.080	0.190

Four mainly diffraction peaks (111), (101), (201) and (103) were used to evaluate the preferred orientation. The calculated texture coefficients TC (hkl) for the three thin films are gathered in Table 2. From these results, it can be observed that all orientations except (111) show a texture coefficient in the range 0< TC (hkl) <1 for different sulphidisation temperature, indicating a lack of the grain orientation in those directions, while the very high TC (111) value confirmed the larger abundance of crystallites to grew in (111) orientation. However, we find not a significant correlation between TC (hkl) values and the sulphidisation temperature.

The quantitative XRD method has been used to estimate structural parameters such as crystallite size, microstrain, lattice parameter and dislocation density, which are important parameters that allows to estimate the technical application of the new semiconductor material.

Grain size has been estimated from the width of the peak, using Debye–Scherrer formula [43]:

$$D = \frac{k\lambda}{\beta \cos(\theta)} \quad (2)$$

where, D is the diameter of the crystallites, *k* is the Scherrer constant, λ is the wavelength of CuK_α, β is the angular line width at half-maximum intensity in radians and θ is the Bragg angle.

The microstrain (ε) and dislocation density (δ) have been estimated using the following standard relations [44]:

$$\varepsilon = \frac{\beta}{4tg\,\theta} \qquad (3)$$

$$\delta = \frac{1}{D^2} \qquad (4)$$

The crystallite sizes of the SnS films calculated for different sulphidisation temperatures are summarized in Table 3. A decrease in the crystallite size from 1782.92 Å to 826,9 Å can be observed when the sulphidisation temperature increases from 250 °C to 400 °C. While the lattice strain and dislocation density are inversely proportional to the crystallite size and accordingly, ε and δ have increased when the sulphidisation temperature has raised from 250 °C to 400 °C (Table 3).

The decrease in grain size with increasing in sulphidisation temperature might be due to some breaking in crystal causing the formation of smaller grains on the surface, which affects the microstructure properties of the film. Similar kind of results has been reported by Devika [45], which has explained it by the fragmentation of clusters of crystallites.

Table 3. Micro structural properties of SnS thin films

Temperatures (°C)	**<D>moy (Å)**	**<δ>moy (m^2)**	**<ε>moy**
250	1782,9186	4,80E+13	0,00079
300	1603,1187	4,31E+13	0,00079
400	826,9045	1,53E+14	0,00152

Indeed, this fact is widely related to some deterioration in the crystallinity of the film, causing the occurrence of voids in the layers that was confirmed by the increase in microstrain values, involving by the increase of the number of defects in the film. Moreover, the increase in sulphidisation temperature leads to a higher thermal stress created into the films [46], which is manifested by a maximum value of both ε and δ. This indicates that the increase in sulphidisation temperature in our case, provoke an increase of the perturbation into the crystal, leading to a greater lattice imperfection.

This explanation could be enhanced by a degradation in the film crystallinity that is evidenced by the decrease in the intensity of the preferred orientation (111) peak when temperature raised

to 400 °C (Figure 2). Therefore, the distinctly smaller values of ε and δ found for the film deposited at 250 °C are a good indication of the lower amount of defects into the film.

3.2 Morphological study

Figure 4 shows Scanning electron microscopy (SEM) micrographs of the tin seed and the SnS layers deposited in the temperature range 250-400 °C. An overview to the different micrographs reveals that the film morphology is significantly affected by the change of the sulphidisation temperature. As shown, the film deposited at 250 °C has a flake-shaped morphology, with irregularly oriented elements tightly bonded together, exhibiting nearly equal size. The SEM micrographs of the films deposited at 300 and 400 °C show that the surfaces of these films seem to be porous and exhibiting irregular round shaped grains with light regions forming a dense network.

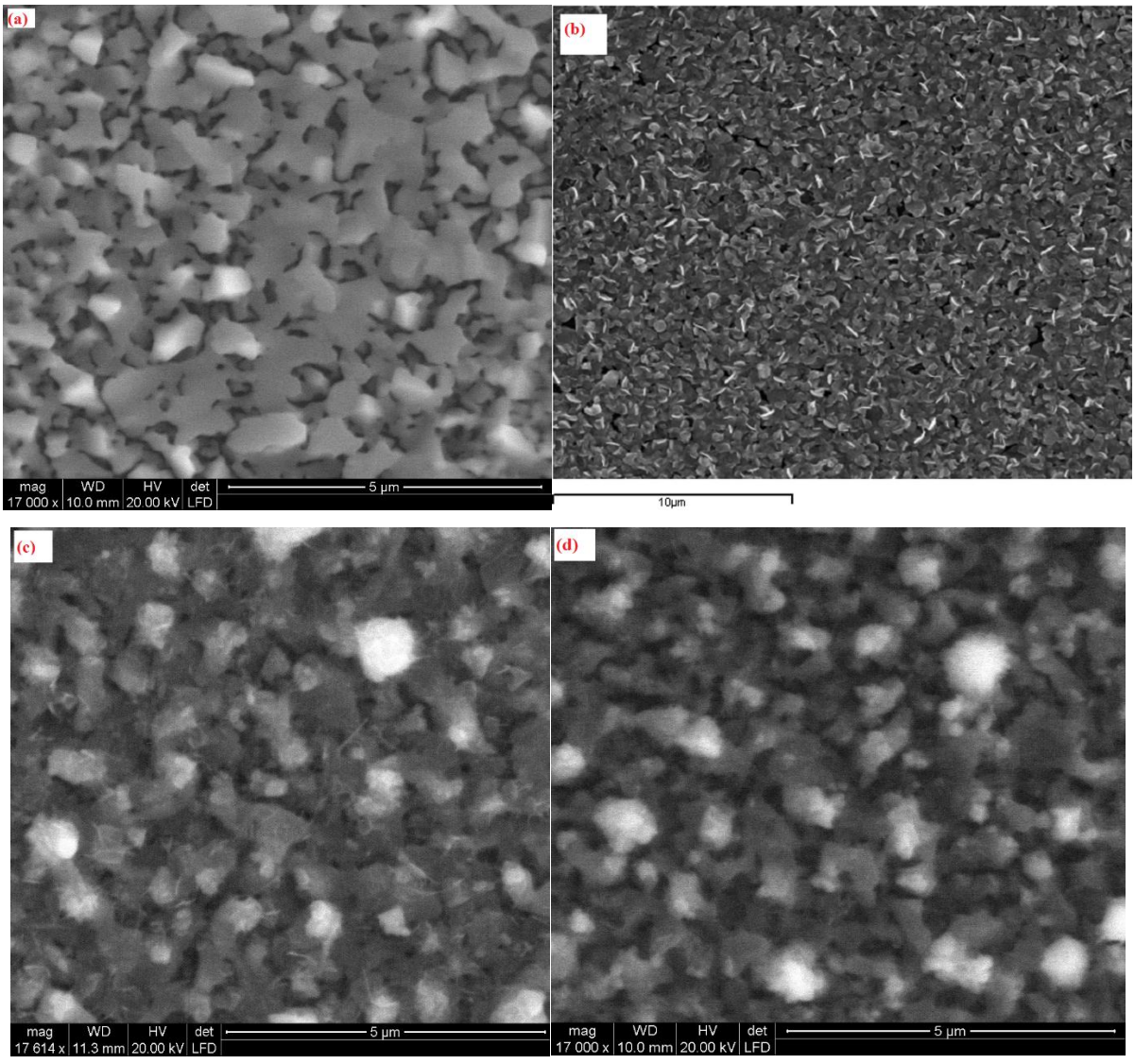

Fig. 4. SEM images of Sn films deposited on glass substrate (a), and SnS films deposited at: (b) 250 °C, (c) 300 °C, (d) 400 °C.

It is also worth noting that the growth tendency of the film allows to pass from flat to granular surface as the sulphidisation temperature increase. This can be due to the fact that some grains have changed its growing orientation when increasing temperature, which can be proved by the decrease of (111) orientation peak in XRD analysis. Therefore, this granular morphology of the films deposited at 300 and 400 °C accompanied by a porous aspect, increase the possibility of forming voids and pinholes, which increase, therefore, the number of defaults inside the films. This observation is in agreement with our microstructural results.

The thickness of the films deposited have been estimated using the cross section SEM image and have found to be equal to 375.3, 408 and 413.8 nm at 250, 300 and 400 °C respectively.

3.3 Raman analysis

To detect and identify materials in trace amounts into the films, a Raman microscopy has been used in the range of 50-550 cm^{-1} at room temperature. Raman spectra recorded for the samples deposited at 250, 300 and 400 °C are shown in Figure 5. The spectra recorded for the film deposited at 250 °C include a prominent band located at 189 cm^{-1}, that can be assigned to SnS phase, according to the predicted data of the orthorhombic tin monosulfide crystal [47]. Two other less prominent SnS modes at 162 and 221 cm^{-1} have been also observed; confirming that the existing phase is the pure tin monosulfide [47]. Increasing temperature to 300 °C, a weaker band different to those related to SnS phase appears at 214 cm^{-1}, suggesting the presence of a minor SnS_2 phase [48]. This occurrence has been manifested in XRD pattern by a decrease in the preferred orientation intensity.

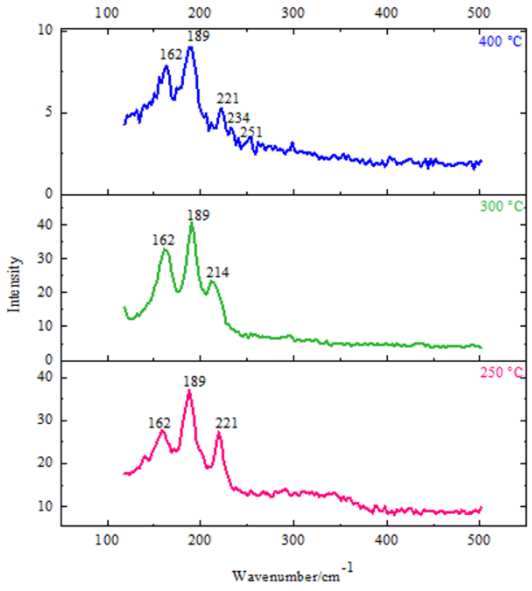

Fig. 5. Raman pattern for the SnS thin films deposited at 250, 300 and 400 °C.

When reaching 400 °C, new Raman phonon modes appear besides those present in the other spectra: Shoulder bands located at 251 and 234 cm^{-1} indicate the formation of a third new phase, the Sn_2S_3, at high temperature [49].

Note that the three samples showed that the prominent bands are those of SnS phase, which indicates that SnS is the major phase present in spite of the appearance of other phases. This fact is in accordance to XRD results where the (111) orientation is the preferred orientation even at high temperatures. Hence, the decrease in the preferred orientation is accompanied with new phase formation.

3.5 Optical properties

The optical transmittance (T%) and reflectance (R%) spectra of the three tin sulfide thin films have been recorded in the wavelength range 500-2500 nm. Results are shown in Figures 6 and 7 respectively.

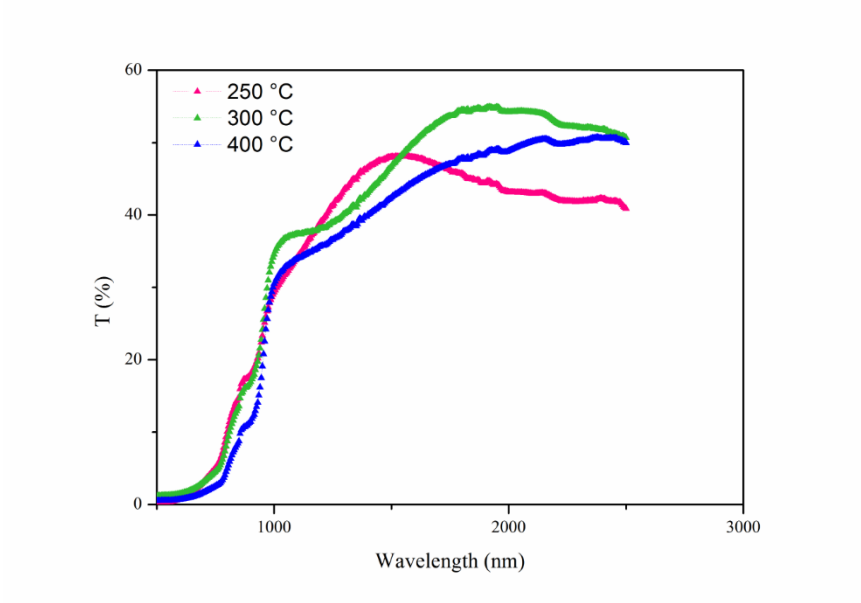

Figure 6. Optical Transmission spectrum for SnS films deposited at 250, 300 and 400 °C.

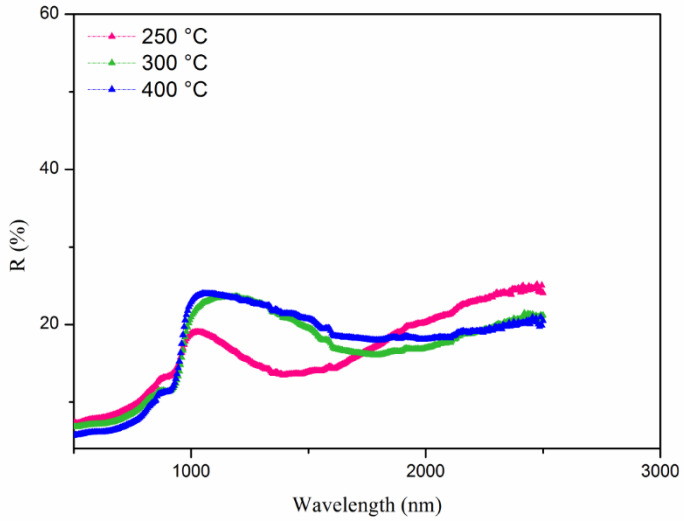

Figure 7. Optical Reflection spectrum for SnS films deposited at 250, 300 and 400 °C.

All the films deposited have practically the same average transmittance in the visible region. However, in the Infrared region the films have dissimilar behaviors as a function of the wavelength. When increasing the wavelength, the film deposited at 250 °C reach a maximum of transmittance at $\lambda \approx 1500$ nm, then returns to decrease slowly to ≈ 40 %, while for the film deposited at 300 °C, some interference has been shown in the IR region, reaching the maximum of transmittance at $\lambda \approx 1900$ nm. However with increasing the sulphidisation temperature to 400 °C, the maximum of transmittance has been achieved at a higher wavelength range. So, the

peak position related to the maximum of transmittance shifts towards larger wavelength values with the increase of sulphidisation temperature.

Analyzing the reflectance curve, samples deposited at different temperatures present similar behavior, reaching a maximum of reflectance at 1000 nm. That is ≈ 18% for the sample deposited at lower temperature and in the range of 22-25 % for the as deposited at higher temperatures. It is noticeable that the reflectance has been affected by the sulphidisation temperature, it increase with increasing temperature from 250 °C to 400 °C.

Such behavior suggests that both transmittance and reflectance of the films could be affected by the increase of the film thickness.

To assess the ability of these materials to absorb sunlight, absorption coefficient α has been estimated from the transmittance and reflectance data using equation (5) [50], where T is transmittance, R is reflectance, and d is the film thickness.

$$\alpha = \frac{1}{d} Ln \frac{(1-R)^2}{T} \qquad (5)$$

The values obtained for the absorption coefficient α in the wavelength range from 250 to 2500 nm are shown in figure 8.

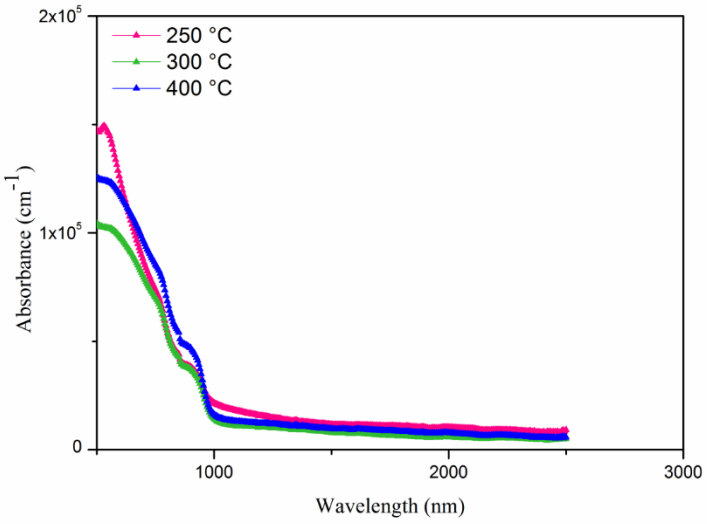

Figure 8. Optical absorption spectrum for SnS films deposited at 250 °C, 300 and 400 °C.

It is clearly observed that all specimens exhibit a high absorption coefficient in the order of 10^5 cm^{-1}, stretching from visible to the near infra-red region which means that all of them behaves

as good absorbing materials, with high ability to convert sunlight. The higher value of α corresponds to the film that exhibit the best crystallinity and pure SnS phase. The decrease of absorbance illustrated in Figure 8 for samples deposited at higher temperatures could be related to the presence of more defects inside the film.

The optical band gap has been determined according the theory of Tauc and Abeles [51], using expression (6),

$$(\alpha h\upsilon) = A(h\upsilon - E_g)^n \qquad (6)$$

where υ is the frequency of the incident photon, h is the Planck' constant, α is the optical absorption coefficient, *n* is equal to ½, 2, 3/2 and 3 for the direct allowed, indirect allowed, direct forbidden and indirect forbidden transitions, respectively. Since in tin sulfide can exist different types of transition, the n value has been determined without any pre-supposing type of transition. The best straight line has been obtained for n=1/2 for all the deposited films, indicating that these materials exhibit a direct allowed transition.

The optical band gap energy has been estimated using the Tauc plot of $(\alpha h\upsilon)^2$ versus the photon energy (hυ), through the extrapolation of the linear portion of the plot to the X base line.

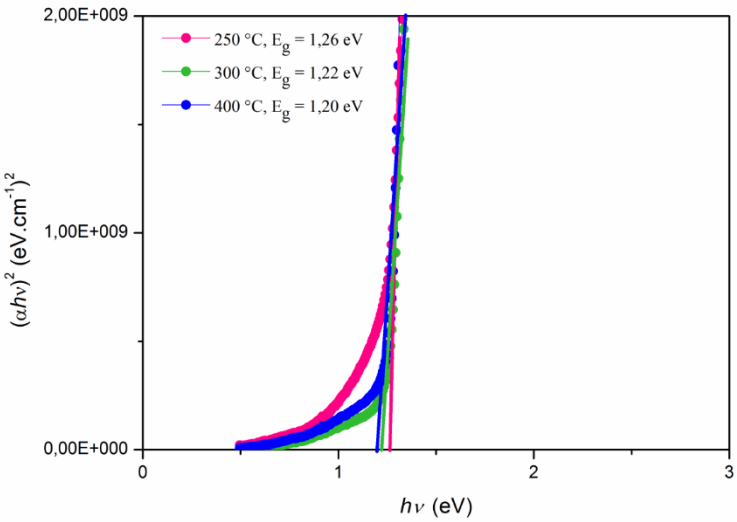

Figure 9. Tauc plot $(\alpha h\upsilon)^2$ vs photon energy (hυ) for SnS films deposited at 250◦C, 300 °C and 400 °C.

The intersection indicates that the values of the band gap energy decrease slightly with increase in sulphidisation temperature. Thus, the film deposited at lower temperature has a band gap

energy of 1.26 eV, and this values decrease to 1.22 eV at 300 °C, reaching 1.20 eV for the higher sulphidisation temperature. This slight difference in the values can be related to the experimental error, but at the same time, the samples are different from the point view of structural properties, as well as, transmittance and reflectance behavior. Therefore, it may be that the effect of more than one factor are responsible of those close Eg values.

It is remarquable that the Eg result has also a meaningful relation with the change of film thickness. Another reason that can explain this decrease in energy band gap are the structural changes suggested by the Raman results, which indicated the formation of other tin sulphide phases as SnS_2 and Sn_2S_3. These results can also be supported by the microstructural observations, relating the decrease of E_g to the increase of the number of defects inside the films. This type of behavior has been observed by other investigators and it has been explained by the increase of the density-localized states in the band gap [52].

The optical band gap energy estimated is larger than that reported by Albers et al. [53] (1.07 eV) and Alpen et al. [48] (1.15 eV) for single-crystal samples, but corresponds well to the reported data on single crystal [36] and polycrystalline films grown by other deposition techniques. Tanusevski [54] obtained optical band gaps of 1.4 eV and 1.38 eV for amorphous and crystalline SnS films grown by CBD technique and showed that the values do not change by thermal treatment. Reddy et al. [55] reported a direct band gap of 1.37 eV for SnS films grown by thermal co-evaporation. Otherwise, these differences in the optical constant is related to the influence of different factors such as the thickness of the films, grain size, surface roughness, mixed tin sulfide phases, presence of vacancies or defects, porosity of the films.

One possible approach to get some information about the smoothness of the surface is to calculate the extinction coefficient using the relation [56]:

$$K = \frac{\alpha\lambda}{4\pi} \qquad (7)$$

where α is the optical absorption coefficient and λ is the wavelength. Figure 10 shows the spectral variation of extinction coefficient k as a function of wavelength in the range of 500–2500 nm.

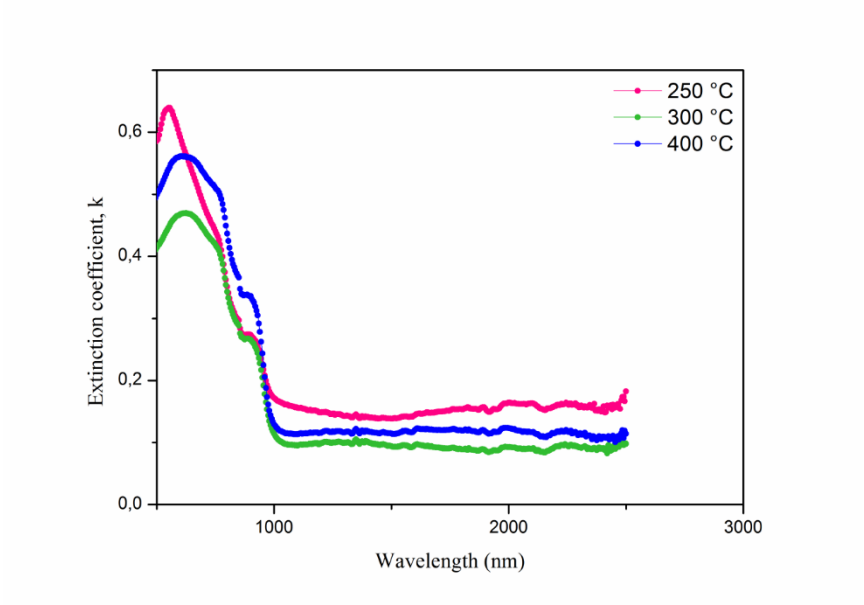

Figure 10. Variation of extinction coefficient (k) with wavelength for SnS thin films deposited at 250 °C, 300 °C and 400 °C.

Figure 10 illustrates that all specimens exhibit the same curves trends, showing a significant peak in the visible region related to the maximum values of k, then decreasing notably when increasing the wavelength until they becomes almost constant for wavelengths higher than 1000 nm.

The higher value of k (0.64) has been obtained for the film deposited at 250 °C around 600 nm. The change in k values with the variation of the sulphidisation temperature is marginal and it can be attributed to the surface morphology changes. Thus, the lower k values of the film deposited at 300 °C is an obvious consequence of the higher surface smoothness of the film and is a key factor for his performance as an optical material. Subsequently the lower values of k at $\lambda \geq$ 1000 nm suggests that the deposited films can be useful in photonic technology at higher wavelengths.

The refractive index is a characteristic parameter of the semiconductor materials, related to the local field within the material. The estimated refractive index n for the tin sulfide films grown at different sulphidisation temperature, evaluated using expression (8) [57], were plotted in Figure 11 as a function of wavelength in the range of 500-2500 nm.

$$n = \frac{1+R}{1-R} + \sqrt{\left[\frac{4R}{(1-R)^2} - K^2\right]} \qquad (8)$$

where R is the optical reflectance and K the extinction coefficient.

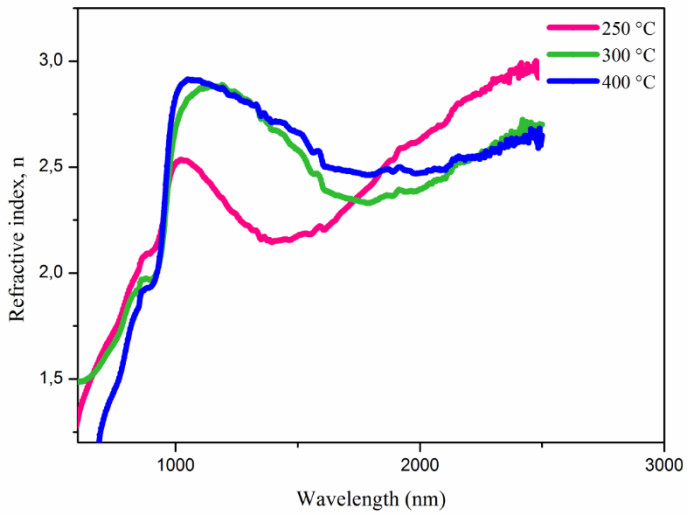

Figure 11. Refractive index of SnS films deposited at 250◦C, 300 °C and 400 °C.

Figure 11 shows that all samples exhibit a similar behavior: firstly, all curves rise rapidly reaching a maximum at 1000 nm, then decreasing in the middle wavelength range and they return to increase at higher wavelength values. The initial drastic increase of *n* for all the layers indicates that the material underwent a swift change in the absorption [58]. The lowest value of n is observed for the sample deposited at 250 °C this lower value is a significant indicator of the porosity of this film, compared to those deposited at higher sulphidisation temperature, which allows considering it as a suitable optical material for optoelectronics devices [59], as well as a promising gas sensing material. However, all the deposited films reach the maximum (n_{max}) around 1050 nm. In this wavelength region, it is obviously observed that n increase monotonically with increasing the film thickness, supporting the interpretation of Mortezaali et al. [60],that related this behavior to a worthy change in the structure as grain boundaries, porosity and roughness. It is also presumably that this change in n is consistent with the microstructure results, in fact the film that shows the lowest n value exhibit the best crystallinity. Since the n is substantially linked with the E_g variation, it can be clearly noticed that a larger band gap energy has a lower n values and conversely. In fact, this observation indicates that the difference between these values and those reported in previous works [56, 58] may be due to structural differences, or to the growth rate of the material, which leads mainly to changes in the optical performance of the material.

3.6 Dielectric characterizations

The research on the field of the optoelectronic material require the determination of the dielectric constant, which is an important parameter directly related to the polarizability of any material. The dielectric constant of the deposited films has been estimated from the relation [61]:

$$\varepsilon = \varepsilon_1 + i\varepsilon_2 \qquad (9)$$

where, the real and imaginary constants have been calculate respectively using the following expressions:

$$\varepsilon_1 = n^2 - k^2 \qquad (10)$$

$$\varepsilon_2 = 2nk \qquad (11)$$

The respective values obtained for theses parameters are shown in Figure 12. Both real and imaginary parts have the same behavior as a function of the photon energy for the three layers analyzed.

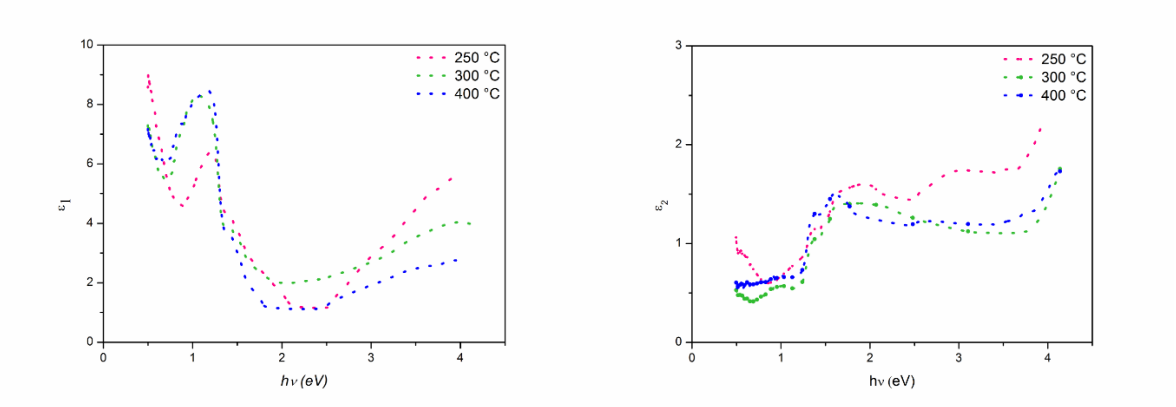

Figure 12. Plot of photon energy dependence of real (a) and imaginary (b) dielectric parts of the SnS thin films deposited at 250◦C, 300 °C and 400 °C.

The real part of the dielectric constant reached the maximum value for a photon energy of 1.3 eV, and a minimum value in the range of 2-2.5 eV, which indicates that the material is slower for low energy photons. However, the imaginary part of the dielectric constant increases with increasing in the photon energy, which depends on the states of the films. The emergence of

some peaks in both shapes of the real and imaginary dielectric spectra can be explained by the interaction between the photons and electrons at the film surface.

Thereby, taking into consideration the dependence of the dielectric constant on n and k parameters, it is possible to avow that both real and imaginary parts have been affected by the same set of factors that affected n and k as the film thickness, grain boundaries, porosity, dislocation density.

Table 4 summarizes the optical parameters obtained in the present work in comparison to those given by other workers.

Table 4. Optical properties of SnS thin films prepared by different techniques.

α (cm^{-1})	E_g (eV)	k	n		
$1.5\ 10^5$	1.26	0.64	2.55	250 °C	Present work
10^5	1.22	0.47	2.8	300 °C	
$1.2\ 10^5$	1.20	0.56	2.9	400 °C	
$> 10^4$	1.3 - 1.41	0.24 - 0.13	2.72-3.24	[62]	
$> 10^4$	1.3 - 1.32	0.06 - 0.12	3.5 - 5.5	[63]	
-	1.9	1.19	3.2	[56]	

The experimental optical data of different tin sulphide thin films such as E_g, n, k, α, show that the physical properties of the deposited films are directly linked to the structural considerations.

Conclusion

The present study has shown a low cost and effective way for successfully deposit SnS thin-film by CVD process using Triphenylphosphine sulfide as a precursor. XRD, SEM, and Raman analysis were used to study the effect of the sulphidisation temperature on crystallinity, chemical composition and surface morphology of thin films. It has been found that the films were polycrystalline in orthorhombic phase, and exhibit a (111) preferential orientation. Microstructural parameters such as crystallite size, strain and dislocation density were estimated as a function of the sulphidisation temperature. The Raman analysis indicate that the films

deposited at 250 °C presented only the tin monosulfide phase, contrariwise to those deposited at 300 and 400 °C, which contains others phases such as SnS_2 and Sn_2S_3.

Optical results show that the films deposited have a high absorption coefficient in the order of 10^5 cm^{-1} in the visible region, and exhibit a direct allowed transition with a band gap ranging from 1.20 to 1.26 eV, which allows this semiconductor to be useful for the fabrication of photovoltaic and optoelectronic devices. The low-n and k values found are both important keys for a good optical performance of the SnS films deposited.

Acknowledgements

Authors are very much thankful to Pr. E. Llobet for accepting the internship in his Research Group at the Department of Electronic, Electrical and Automatic Engineering of University Rovira i Virgili in Tarragona, Spain. Also we wishes to acknowledge Pr. A. Boukhachem for his insightful remarks and University of Tunis El-Manar for "the Alternance Bourse" granted.

References

[1] D. Yoo, M. S. Choi, S. C. Heo, C. Chung, D. Kim, C. Choi, Structural, Optical and Chemical Analysis of Zinc Sulfide Thin Film Deposited by RF-Mganetron Sputtering and Post Deposition Annealing, Met. Mater. Int. 19 (2013) 1309–1316.

[2] A. N. Rodriguez, M. T. S. Nair, P. K. Nair, Structural, optical and electrical properties of chemically deposited silver sulfide thin films, Semicond. Sci. Technol. 20 (2005) 576–585.

[3] A. M. Salem, M. S. Selim, Structure and optical properties of chemically deposited Sb2S3 thin films, J. Phys. D: Appl. Phys. 34 (2001) 12–17.

[4] R. Gonzàlez-Lùa, J. Escorcia-Garcia, D. Perez-Martinez, M. T. S. Nair, J. Campos, P. K. Nair, Stable Performance of Chemically Deposited Antimony Sulfide-Lead Sulfide Thin Film Solar Cells under Concentrated Sunlight, ECS J. Solid State Sci. Technol. 4 (2015) Q9–Q16.

[5] A. B. F. Martinson, S. C. Riha, E. Thimsen, J. W. Elam, M. J. Pellin, Structural, optical, and electronic stability of copper sulfide thin films grown by atomic layer deposition, Energy Environ. Sci. 6 (2013) 1868.

[6] S. S. Rao, C. V. V. M. Gopi, S-K. Kim, M-K. Son, M-S. Jeong, A. D. Savariraj, K. Prabakar, H-J. Kim, Cobalt sulfide thin film as an efficient counter electrode fordye-sensitized solar cells, Electrochim. Acta. 133 (2014) 174–179.

[7] J. Cardoso, O. GomezDaza, L. Ixtlilco, M.T.S. Nair, P.K. Nair, Conductive copper sulfide thin films on polyimide foils, Semicond. Sci. Technol. 16 (2001) 123–127.

[8] A. Gaiardo, P. Bellutti, S. Gherardi, G. Zonta, B. Fabbri, A. Giberti, V. Guidi, C. Malagù, Tin (IV) Sulfide chemoresistivity: a possible new gas sensing material, AISEM, Annual Conference, XVIII (2015).

[9] X. Xin, M. He, W. Han, J. Jung, Z. Lin, Low-Cost Copper Zinc Tin Sulfide Counter Electrodes for High-Efficiency Dye-Sensitized Solar Cells, Angew. Chemie Int. Ed. 50 (2011) 11739–11742.

[10] S. M. Yang, C. H. Huang, J. Zhai, Z. S. Wang, J. Jiang, High photostability and quantum yield of nanoporous TiO2 thin film electrodes co-sensitized with capped sulfides, J. Mater. Chem. 12 (2002) 1459–1464.

[11] A. A. Sagade, R. Sharma, Copper sulphide (CuxS) as an ammonia gas sensor working at room temperature, Sensors Actuators, B Chem. 133 (2008) 135–143.

[12] O. V. Salata, P. J. Dobson, S. Sabesan, P. J. Hull, J. L. Hutchison, Preparation of nanoparticulate CdS films suitable for opto-electronic device applications, thin solid films 288 (1996) 235–238.

[13] L.-X. Shao, K.-H. Chang, H.-L. Hwang, Zinc sulfide thin films deposited by RF reactive sputtering for photovoltaic applications, Appl. Surf. Sci. 212-213 (2003) 305–310.

[14] K. W. Nebesny, G. E. Collins, P. A. Lee, L. K. Chau, J. Danziger, E. Osburn, N. R. Armstrong, Organic/Inorganic Molecular Beam Epitaxy: Formation of an Ordered Phthalocyanine/SnS2 Heterojunction, Chem. Mater. 3 (1991) 829–838.

[15] J. Aguilar-Hernandez, G. Contreras-Puente, A. Morales-Acevedo, O. Vigil-Galàn, F. Cruz-Gandarilla, J. Vidal-Larramendi, et al., Photoluminescence and structural properties of cadmium sulphide thin films grown by different techniques, Semicond. Sci. Technol. 18 (2003) 111–114.

[16] K. T. Ramakrishna Reddy, P. Purandar Reddy, R. W. Miles, P. K. Datta, Investigations on SnS films deposited by spray pyrolysis, Opt. Mater. 17 (2001) 295–298.

[17] M. Gunasekaran, M. Ichimura, Photovoltaic cells based on pulsed electrochemically deposited SnS and photochemically deposited CdS and $Cd_{1-x}Zn_xS$, Sol. Energy Mater. Sol. Cells. 91 (2007) 774–778.

[18] D. Avellaneda, G. Delgado, M. T. S. Nair, P. K. Nair, Structural and chemical transformations in SnS thin films used in chemically deposited photovoltaic cells, Thin Solid Films. 515 (2007) 5771–5776.

[19] B. Ghosh, M. Das, P. Banerjee, S. Das, Fabrication of vacuum-evaporated SnS/CdS heterojunction for PV applications, Sol. Energy Mater. Sol. Cells. 92 (2008) 1099–1104.

[20] M. M. El-Nahass, H. M. Zeyada, M. S. Aziz, N. A. El-Ghamaz, Optical properties of thermally evaporated SnS thin films, Opt. Mater. 20 (2002) 159–170.

[21] A. Ortiz, J. C. Alonso, M. Garcia, J. Toriz, Tin sulphide films deposited by plasma-enhanced chemical vapour deposition, Semicond. Sci. Technol. 11 (1996) 243–247.

[22] P. Marchand, I. A. Hassan, I. P. Parkin, C. J. Carmalt, Aerosol-assisted delivery of precursors for chemical vapour deposition: expanding the scope of CVD for materials fabrication, Dalt. Trans. 42 (2013) 9406.

[23] G. Valiukonia, D. A. Guseinova, G. Krivitb, A. Sileika, Optical Spectra and Energy Band Structure of Layer-Type $A^{IV}B^{V1}$ Compounds, phys. stat. sol. 135, (1986) 299-307.

[24] N. K. Reddy, K. T. R. Reddy, G. Fisher, R Best, P K Dutta, The structural behaviour of layers of SnS grown by spray pyrolysis, J. Phys. D: Appl. Phys. 32 (1999) 988–990.

[25] T. G. Hibbert, M. F. Mahon, K. C. Molloy, L. S. Price, I. P. Parkin, Deposition of tin sulfide thin films from novel, volatile (fluoroalkythiolato)tin (IV) precursors, J. Mater. Chem., (2001), 11, 469-473.

[26] A. Gibertia, A. Gaiardoa, B. Fabbria, S. Gherardia, V. Guidia, C. Malagùa, P. Bellutti, G. Zonta, D. Casottia, G. Cruciania, Tin(IV) sulfide nanorods as a new gas sensing material, Sensors and Actuators B 223 (2016) 827–833.

[27] P. Boudjouk, D. J. Seidler, S. R. Bahr, G. J. McCarthy, The aerosol assisted chemical vapour deposition of SnSe and Cu_2SnSe_3 thin films from molecular precursors, Chem. Mater. 6 (1994) 2108-2112.

[28] S. S. Hegde, A. G. Kunjomana, K. Ramesh, Microhardness studies of vapour grown tin (II) sulfide single crystals, AIP Conf. Proc. 1665 (2015) 100010.

[29] K. T. Ramakrishna Reddy, N. Koteswara Reddy, R. W. Miles, Photovoltaic properties of SnS based solar cells, Sol. Energy Mater. Sol. Cells. 90 (2006) 3041–3046.

[30] S. K. Arora, D. H. Patel, M. K. Agarwal, Electrical and optical behaviour of vapour-grown SnS_2 crystals, J. Mater. Sci. 29 (1994) 3979–3983.

[31] U. V. Alpen, J. Fenner, E. Gmelin, Semiconductors of the type $Me^{II}Me^{IV}S_3$, Mat. Res. Bull. 10 (1975), 175-180.

[32] M. A. Green, The Path to 25% Silicon Solar Cell Efficiency: History of Silicon Cell Evolution, Prog. Photovolt: Res. Appl. 17 (2009) 183–189.

[33] Y. J. Yang, B. J. Xiang, A simple synthesis of SnS nanoflakes at ambient conditions, Appl. Phys. A, 83 (2006) 461–463.

[34] N. K. Reddy, K.T. R. Reddy, Preparation and characterisation of sprayed tin sulphide

films grown at different precursor concentrations, Mater. Chem. Phys. 102 (2007) 13–18.

[35] M. Ristov, G. Sinadinovski, I. Grozdanov, M. Mitreski, Chemical deposition of tin (II) sulphide thin film, Thin Solid Films. 173 (1989) 53–58.

[36] P. Kevin, D.J. Lewis, J. Raftery, M. A. Malik, P. O'Brien, Thin Films of SnS by Aerosol-Assisted Chemical Vapour Deposition (AACVD) Using Tin(II) Dithiocarbamates as Single-Source Precursors, J. Cryst. Growth. 415 (2015) 93–99.

[37] P. Boudjouk, D. J. Seidler, D. Grier, G. J. Mccarthy, Benzyl-Substituted Tin Chalcogenides. Efficient Single-Source Precursors for Tin Sulfide, Tin Selenide, and $Sn(SxSe_{1-x})$ Solid Solutions, Chem. Mater. 8 (1996) 1189–1196.

[38] P. Boudjouk, D. J. Seidler, S. R. Bahr, G. J. Mccarthy, Bis(tripheny1tin) Chalcogenides as Convenient Precursors to Phase-Pure Binary Semiconductors, Chem. Mater. 6 (1994) 2108–2112.

[39] M. J. Hampden-Smith, T. T. Kodas, Chemical Vapor Deposition of Metals: Part 1. An Overview of CVD Processes, Chem. Vap. Dep. (1995) 8-23.

[40] I. V. Slipukhina, D. M. Bercha, Elementary energy bands in isovalent IV–VI orthorhombic and cubic crystals and their solid solutions, Phys. Stat. Sol. 244 (2007) 650–668.

[41] H. Wiedemeier, F. J. Csillag, The thermal expansion and high temperature transformation of SnS and SnSe, Z. Kristallogr. 149 (1979) 17-29.

[42] M. Caglar, Y. Caglar, S. Ilican, The determination of the thickness and optical constants

of the ZnO crystalline thin film by using envelope method, J. Optoelectron. Adv. Mater. 8 (2006) 1410–1413.

[43] P. Scherrer, Nachrichten von der Gesellschaft der Wissenschaften zu Göttingen, Math. Klasse. (1918) 98–100.

[44] S. Thanikaikarasan, T. Mahalingam, K. Sundaram, A. Kathalingam, Y. Deak Kim, T. Kim, Growth and characterization of electrosynthesized iron selenide thin films, Vacuum. 83 (2009) 1066–1072.

[45] M. Devika, N. K. Reddy, K. Ramesh, K. R. Gunasekhar, E.S.R. Gopal, K.T.R. Reddy, Influence of annealing on physical properties of evaporated SnS films, Semicond. Sci. Technol. 21 (2006) 1125–1131.

[46] T. S. Rao, B. K. Samantharay, A. K. Chaudhuri, Structural characterization of tin selenide thin films, J. Mater. Sci. Lett. 4 (1985) 743–745.

[47] H. R. Chandrasekhar, R. G. Humphreys, U. Zwick, M. Cardona, Infrared and Raman spectra of the IV-VI compounds SnS and SnSe, Phys. Rev. B. 15 (1977) 2177–2183.

[48] I. P. Parkin, L. S. Price, T. G. Hibbert, K. C. Molloy, The first single source deposition of tin sulfide coatings on glass: aerosol-assisted chemical vapour deposition using [Sn(SCH2CH2S)2], J. Mater. Chem. 11 (2001) 1486–1490.

[49] A.T. Kana, T.G. Hibbert, M.F. Mahon, K.C. Molloy, I.P. Parkin, L.S. Price, Organotin unsymmetric dithiocarbamates: synthesis, formation and characterisation of tin(II) sulfide films by atmospheric pressure chemical vapour deposition, Polyhedron 20 (2001) 2989–2995.

[50] N. Barreau, S. Marsillac, J. C. Bernède, T. Ben Nasrallah, S. Belgacem, Optical Properties of Wide Band Gap Indium Sulphide Thin Films Obtained by Physical Vapor Deposition, phys. stat. sol. 184 (2001) 179–186.

[51] J. Tauc, A. Menth, States in the Gap, J. Non. Cryst. Solids. 8-10 (1972) 569-585.

[52] C. Mahendran, N. Suriyanarayanan, Physica B: Condens. Matter 405 (2010) 2009.

[53] W. Albers, C. Haas, F. V. D. Maesen, The Preparation and the Electrical and Optical Properties of SnS Crystals, J. Phys. Chem. Solids. 15 (1960) 306-310.

[54] A. Tanusevski, Optical and photoelectric properties of SnS thin films prepared by chemical bath Deposition, Semicond. Sci. Technol. 18 (2003) 501–505.

[55] N. K. Reddy, K. Ramesh, R. Ganesan, K. T. R. Reddy, K. R. Gunasekhar, E. S. R. Gopal, Synthesis and characterisation of co-evaporated tin sulphide thin films, Appl. Phys. A Mater. Sci. Process. 83 (2006) 133–138.

[56] D. Beena, K.J. Lethy, R. Vinodkumar, V.P. M. Pillai, V. Ganesan, D.M. Phase, S.K. Sudheer, Effect of substrate temperature on structural, optical and electrical properties of pulsed laser ablated nanostructured indium oxide films, Appl. Surf. Sci. 255 (2009) 8334–8342.

[57] N. M. Gasanly, Effect of isomorphic atom substitution on the refractive index and oscillator parameters of $TlInS_{2x}Se_{2(1-x)}$ ($0.25 \leq x \leq 1$) layered mixed crystals, Cryst. Res. Technol. 45 (2010) 1141-1144.

[58] Y. Ji, Y. Ou, Z. Yu, Y. Yan, D. Wang, C. Yan, L. Liu, Y. Zhang, Y. Zhao, Effect of film thickness on physical properties of RF sputtered In 2S3 layers, Surf. Coat. Tech. 276 (2015) 587–594.

[59] E. F. Schubert, J. K. Kim, J.-Q. Xi, Low-refractive-index materials: A new class of optical thin-film materials, Phys. Status Solidi. 244 (2007) 3002–3008.

[60] A. Mortezaali, O. Taheri, Z.S. Hosseini, Thickness effect of nanostructured ZnO thin films prepared by spray method on structural, morphological and optical properties, Microelectronic Eng, 151 (2016), 19-23.

[61] R. Sahraei, A. Daneshfar, A. Goudarzi, S. Abbasi, M. H. M. Ara, F. Rahimi, Optical properties of nanocrystalline ZnS:Mn thin films prepared by chemical bath deposition method, J Mater Sci Mater Electron. 24 (2013) 260–266.

[62] S. Gedi, V. R. M. Reddy, C. Park, J. Chan-Wook, R. Reddy, K. T, Comprehensive optical studies on SnS layers synthesized by chemical bath deposition, Opt Mater,42 (2015) 468-475.

[63] P. A. Nwofel, K. T. R. Reddy, J. K. Tan, I. Forbes, R. W. Miles, Thickness dependent optical properties of thermally evaporated SnS thin films, Phys. Procedia, 25 (2012) 150-157.